DRAFT VERSION JANUARY 16, 2014
Preprint typeset using LaTeX style emulateapj v. 5/2/11

arXiv:1401.3340v1 [astro-ph.GA] 14 Jan 2014

PROBING THE LARGE AND MASSIVE CGM OF A GALAXY AT $Z \sim 0.2$ USING A PAIR OF QUASARS[1]

SOWGAT MUZAHID[2]

Draft version January 16, 2014

ABSTRACT

We present analysis of two O VI absorbers at redshift $z_{\rm abs}$ = 0.227, detected in the spectra of two closely spaced QSO sightlines (Q 0107−025 **A** and **B**), observed with the Cosmic Origins Spectrograph (COS) on board the *Hubble Space Telescope* (*HST*). At the same redshift, presence of a single bright ($\sim 1.2 L_\star$) galaxy at an impact parameter of $\sim$ 200 kpc (proper) from both the sightlines was reported by Crighton et al. (2010). Using detailed photoionization models we show that the high ionization phases of both the O VI absorbers have similar ionization conditions (e.g. $\log U \sim -1.1$ to -0.9), chemical enrichment (e.g. $\log Z \sim -1.4$ to -1.0), total hydrogen column density (e.g. $\log N_{\rm H}({\rm cm}^{-2}) \sim 19.6 - 19.7$) and line of sight thickness (e.g. $l_{\rm los} \sim$ 600 – 800 kpc). Therefore we speculate that the O VI absorbers are tracing different parts of same large scale structure, presumably the circumgalactic medium (CGM) of the identified galaxy. Using sizes along and transverse to the line of sight, we estimate the size of the CGM to be $R \sim 330$ kpc. The baryonic mass associated with this large CGM as traced by O VI absorption is $\sim 1.2 \times 10^{11} M_\odot$. A low ionization phase is detected in one of the O VI systems with near solar metallicity ($\log Z = 0.20 \pm 0.20$) and parsec scale size ($l_{\rm los} \sim$ 6 pc), possibly tracing the neutral phase of a high velocity cloud (HVC) embedded within the CGM.

Subject headings: galaxies: formation — quasars: absorption lines — quasar: individual (Q 0107−025A, Q 0107−025B)

1. INTRODUCTION

According to current theoretical models, accretion of pristine gas from the intergalactic medium (IGM; Kereš et al. 2005; Dekel et al. 2009; Bouché et al. 2010; Davé et al. 2012) and efficient galactic-scale outflows of metal-enriched gas (Springel & Hernquist 2003; Oppenheimer et al. 2010; Davé et al. 2011a,b) are the two primary factors that govern the formation and evolution of galaxies. Some of the outflowing metal-enriched material eventually returns to galaxies (Oppenheimer et al. 2010). This "baryon cycle" alters the ionization and chemical conditions of the circumgalactic medium (CGM), i.e. gas in the immediate vicinity of galaxies that lies within the dark matter halos. However, due to low density of the CGM gas, direct detection of such a "baryon cycle" remains a big challenge.

The absorption lines observed in the spectra of distant quasars (QSOs) allow us to probe this tenuous CGM (Tumlinson et al. 2011b; Thom et al. 2012; Werk et al. 2013), which is otherwise not visible to us. However, the major drawback of absorption line spectroscopy is that one does not have any information about variations in the physical conditions of the absorbing gas in the direction transverse to the line of sight. Closely spaced QSO pairs (or groups) can provide useful information regarding transverse size and therefore the tomography of the absorber (Bechtold et al. 1994; Dinshaw et al. 1995, 1997; D'Odorico et al. 1998; Rauch et al. 2001; Petry et al. 2006; Crighton et al. 2010).

The resonant transitions of five times ionized oxygen (i.e. O VI$\lambda\lambda$1031,1037) is a useful tracer of low density diffuse gas. The high cosmic abundance of oxygen and high ionization potential (IP = 113.9 eV) provide O VI doublets with immense diagnostic power. O VI absorption is observed in a wide variety of astrophysical environments, e.g. IGM (Tripp et al. 2008; Thom & Chen 2008; Muzahid et al. 2011, 2012), local ISM and Galaxy halo (Savage et al. 2003; Wakker & Savage 2009), HVC (Sembach et al. 2003), CGM (Tumlinson et al. 2011a,b; Kacprzak et al. 2012; Stocke et al. 2013) etc. In particular, in pioneering work, Tumlinson et al. (2011b) have shown that O VI absorption is ubiquitous in the CGM of isolated star forming galaxies. Moreover, this highly ionized CGM gas contains considerable mass that can account for the "missing baryons" in galaxies (see also Tripp et al. 2011).

In this paper we present analysis of two O VI absorbers at redshift $z_{\rm abs}$ = 0.227, detected in the spectra of two closely spaced quasars. Crighton et al. (2010) have identified a bright galaxy at an impact parameter of $\sim$ 200 kpc at the redshift of the absorbers. We use photoionization models to understand the physical conditions of the CGM of the galaxy as probed by the O VI absorption. Moreover, we present a robust estimate of the CGM mass using the model predicted values of metallicity and ionization correction. This paper is organized as follows: after presenting observations and data reduction in section 2, data analysis and photoionization models are presented in section 3. In section 4 we discuss our results and summarize the conclusions. Throughout this paper we adopt an H_0 = 70 km s^{-1}Mpc^{-1}, $\Omega_{\rm M}$ = 0.3 and Ω_Λ = 0.7 cosmology. The relative abundance of heavy elements is taken from Asplund et al. (2009). All the distances given are proper (physical) distances.

2. OBSERVATIONS, DATA REDUCTION AND LINE MEASUREMENT

The well known QSO pair (Q 0107−025A, $z_{\rm em}$ = 0.960; Q 0107−025B, $z_{\rm em}$ = 0.956; hereafter **A** and **B**) were first observed by Dinshaw et al. (1995, 1997) with the *HST*/FOS (Faint Object Spectrograph) on February 1994. Young et al. (2001), subsequently presented observations of another nearby quasar Q 0107−0232 ($z_{\rm em}$ = 0.726). Among

[1] Based on observations made with the NASA/ESA *Hubble Space Telescope*, obtained from the data archive at the Space Telescope Science Institute, which is operated by the Association of Universities for Research in Astronomy, Inc., under NASA contract NAS 5-26555.

[2] The Pennsylvania State University, 413 Davey Lab, University Park, State College, PA 16801, USA

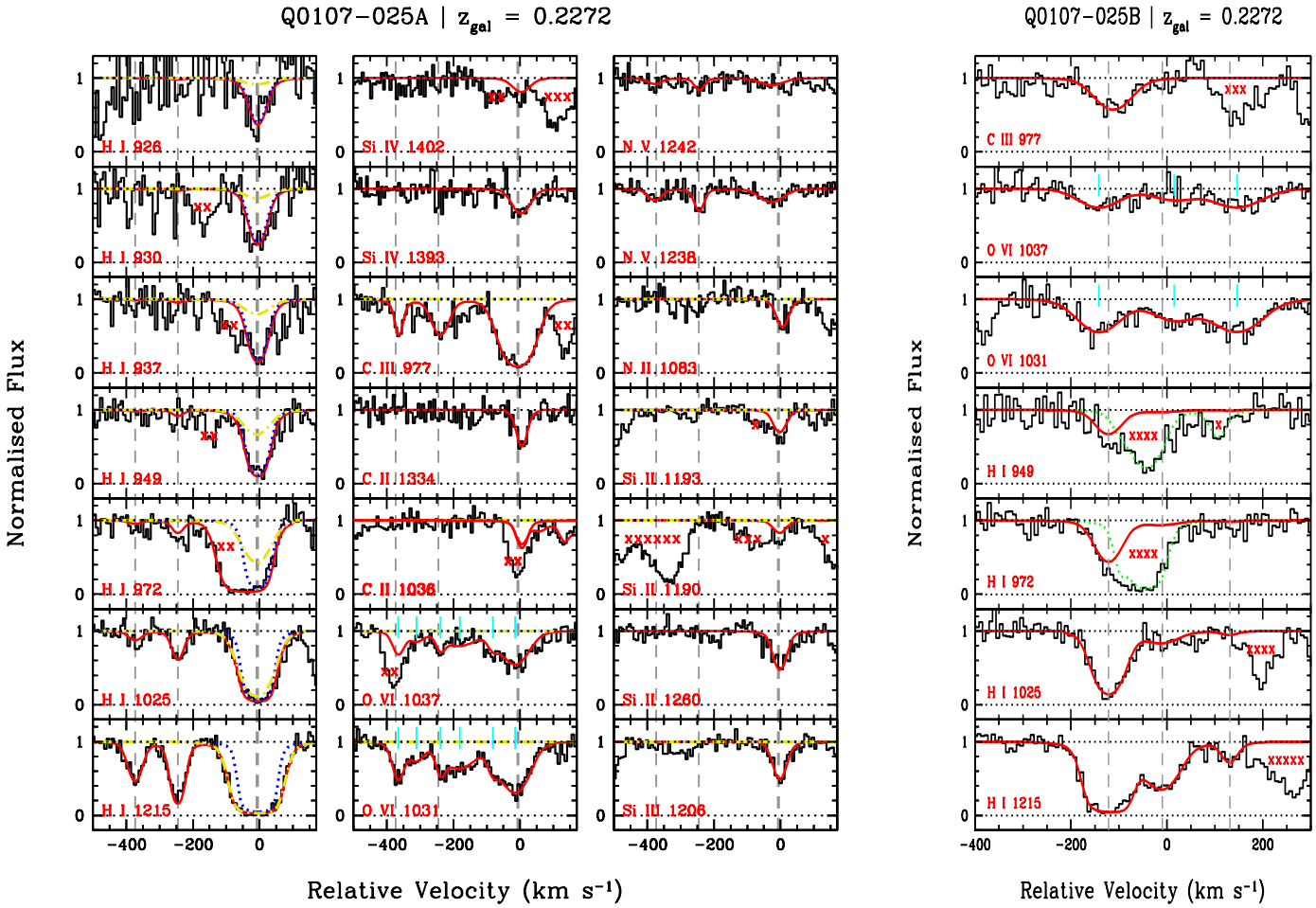

Figure 1. Absorption profiles (black histograms) of different species in the $z_{\rm abs}$ = 0.227 system, detected in the spectrum of **A** (left) and **B** (right), are plotted in velocity. The zero velocity corresponds to the redshift of the galaxy $z_{\rm gal}$ = 0.2272. Best fitting Voigt profiles are shown in smooth (red) curves. The (blue) dotted and (yellow) dot-dashed curves in the Lyman series lines in the left panel show the H I absorption associated with low and high ionization phases respectively. The (blue) dotted profile is dominated by the higher order Lyman series absorption whereas the (yellow) dot-dashed profile is dominated by the shape of Lyα and Lyβ absorption (see text). Component centroids of H I absorption are shown by the dashed vertical lines. The ticks in the O VI panels mark the line centroids of O VI components. Unrelated absorption (blends) are marked by 'x'. The (green) dotted profiles in the right panel represent model for the blend.

these three quasars, the minimum angular separation is between the pair **A** and **B** ($\Delta\theta$ = 1.29 arcmin). This angular separation corresponds to a transverse distance of $\sim$ 280 kpc at $z_{\rm abs}$ = 0.227 for our adopted cosmology. The analysis of Lyα absorbers in this QSO triplet, based on low resolution data, has been presented in several previous papers (e.g., Dinshaw et al. 1995, 1997; D'Odorico et al. 1998; Petry et al. 2006; Crighton et al. 2010). In this paper, we will concentrate on two highly ionized absorbers detected via O VI absorption in medium resolution COS spectra. The third QSO, Q 0107−0232, is observed only with the COS/G160M grating and therefore the spectrum does not cover O VI for the redshift of interest. We thus do not use the spectrum of Q 0107−0232 in our analysis.

The ultraviolet (UV) spectra of Q 0107−025 (**A** and **B**) were obtained using HST/COS during observation cycle-17, under program ID: 11585 (PI: Neil Crighton). These observations consist of G130M and G160M far-UV (FUV) grating integrations at medium resolution of $\lambda/\Delta\lambda \sim 20,000$ and signal-to-noise ratio $S/N \sim 10$ per resolution element in the wavelength range 1134 – 1796 Å. The properties of COS and its in-flight operations are discussed by Osterman et al. (2011) and Green et al. (2012). The data were retrieved from the HST archive and reduced using the STScI CALCOS v2.17.2 pipeline software. The reduced data were flux calibrated. The alignment and addition of the separate G130M and G160M exposures were done using the software developed by the COS team[3]. The exposures were weighted by the integration time while coadding in flux units. The reduced coadded spectra were binned by 3 pixels as the COS data in general are highly oversampled (6 pixels per resolution element). All measurements and analysis in this work were performed on the binned data. While binning improves the S/N of the data, measurements are found to be fairly independent of binning. Continuum normalization was done by fitting the line free regions with a smooth lower order polynomial. For Voigt profile fit analysis, we use non-Gaussian COS line spread function given by Kriss (2011). Multiple transitions (e.g., doublets or Lyman series lines) were always fitted simultaneously to estimate best fitting column densities.

3. ANALYSIS

In total, there are 10 O VI systems detected in both **A** and **B**. However, only two systems (i.e. $z_{\rm abs}$ = 0.227 and 0.399),

[3] http://casa.colorado.edu/∼danforth/science/cos/costools.html

are common to both **A** and **B**. The $z_{\rm abs}$ = 0.227 system is associated with a known bright galaxy (Crighton et al. 2010). But no galaxy information is available for the other system. In this paper we focus on the $z_{\rm abs}$ = 0.227 system as observed in the spectra of **A** and **B**. Detailed analysis of the other system (i.e. $z_{\rm abs}$ = 0.399) with be presented in an upcoming paper by Muzahid et al. (in preparation).

3.1. *System at $z_{\rm abs} = 0.227$ towards* **A** *(system* **1A***)*

Absorption profiles of different species detected in this system are shown in the left panel of Fig. 1. The Lyα and Lyβ absorption clearly show three distinct absorption components spread over $\sim$500 km s^{-1}. The two weak H I components (at relative velocities $v_{\rm rel} \sim -250$ and -400 km s^{-1}) are associated with C III, N V and O VI absorption. The strongest H I component at $v_{\rm rel} \sim 0$ km s^{-1} is associated with low (N II, Si II, C II), intermediate (C III, Si IV) and high (N V and O VI) ionization metal lines. Crighton et al. (2010) report detection of C IV absorption in the HST/FOS spectrum with an observed equivalent width of $W_{\rm obs}(1548) = 0.86 \pm 0.20$ Å. This corresponds to $\log N$(C IV) = 14.24$\pm$0.12, assuming that the line falls on the linear part of the curve of growth. Note that the Si IV absorption is detected only in the Si IVλ1393 transition. The other member of the doublet is blended. Moreover, the Si IVλ1393 line could have contamination from N IIIλ989 absorption from the $z_{\rm abs}$ = 0.7286 system. Therefore the measured N(Si IV) is strictly an upper limit. The O VIλ1037 transition in the blue-most component (i.e. at $v_{\rm rel}\sim -400$ km s^{-1}) is blended with the Lyα forest. Note that C IIλ1036 from $v_{\rm rel}\sim$ 0 km s^{-1}also falls at the same wavelengths. The O VI absorption is spread over $\sim$410 km s^{-1} and show markedly different profile compared to those of low ions. Minimum six Voigt profile components are required to fit the O VI doublets adequately. To simplify our photoionization model, we summed the O VI column densities of three pairs of nearest-neighbor components (see Table 1).

Presence of several unsaturated higher order Lyman series (up to Ly-926) lines in the strongest H I component allows robust determination of N(H I). Lyγ absorption is severely blended with the Galactic Si IIλ1193 absorption. We modelled out the contamination while fitting the Lyman series lines. The column density and the Doppler parameter required to fit the higher order lines (i.e. Lyδ, Ly-937, Ly-930 and Ly-926) cannot fully explain the observed Lyα and Lyβ absorption. The (blue) dotted profile in the velocity plot (see Fig. 1) shows the contribution of the component which dominates the profiles of higher order lines. This component has a Doppler parameter of b(H I) = 26$\pm$3 km s^{-1}. It is evident from the Lyα and Lyβ profiles that we need another component (preferably broad) to produce a reduced $\chi^2\sim$1. The (yellow) dot-dashed profile represents this broad component with b(H I) = 48$\pm$4 km s^{-1}. Because of the presence of multiple ions at different ionization states we focus photoionization model for the component at $v_{\rm rel} \sim 0$ km s^{-1}.

3.1.1. *Photoionization Model for system* **1A**

Photoionization models are run using CLOUDY (Ferland et al. 1998) assuming the absorbing gas (a) has plane parallel geometry, (b) has solar relative abundances (Asplund et al. 2009) for heavy elements and (c) is exposed to the extragalactic UV background (Haardt & Madau 1996) at redshift $z = 0.23$. Here we do not consider the effect of a galaxy/stellar radiation field, as it is negligible at this redshift at a large separation ($\sim$ 100 kpc) from bright ($> L_\star$) galaxies (see e.g. Narayanan et al. 2010). We also note that the candidate galaxy does not show any signs of recent star formation (Crighton et al. 2010).

Table 1
Column densities in the $z_{\rm abs}$ = 0.227 systems towards **A** and **B**

System 1A	$\log N$ (cm^{-2})		
	Velocity ($v_{\rm rel}$) range in km s^{-1}		
Species	(-438 to -267)	(-267 to -118)	(-118 to +150)[d]
H I (High)[a]	13.53$\pm$0.04	14.07$\pm$0.05	15.06$\pm$0.19
H I (Low)[b]			15.92$\pm$0.08
O VI	14.16$\pm$0.20	14.28$\pm$0.28	14.57$\pm$0.23
N V	13.28$\pm$0.11	13.48$\pm$0.07	13.55$\pm$0.08
C IV[c]			14.24$\pm$0.12
Si IV			$<$13.18$\pm$0.08
C III	13.20$\pm$0.11	13.37$\pm$0.05	14.20$\pm$0.05
Si III			12.90$\pm$0.05
C II			13.85$\pm$0.07
Si II			13.04$\pm$0.06
N II			13.88$\pm$0.08
System 1B	$\log N$ (cm^{-2})		
	Velocity ($v_{\rm rel}$) range in km s^{-1}		
Species	(-243 to -56)[d]	(-56 to -74)	(-74 to +231)
H I	14.92$\pm$0.05	13.82$\pm$0.03	13.07$\pm$0.09
O VI	14.24$\pm$0.03	14.01$\pm$0.06	14.30$\pm$0.04
C III	13.44$\pm$0.04	(blended)	(blended)
N V	$<$ 13.50		
Si IV	$<$ 13.25		

Notes – [a]H I associated with high ionization phase. [b]H I associated with low ionization phase. [c]N(C IV) calculated from $W_{\rm obs}$ given in Crighton et al. (2010). [d]photoionization model is done for this clump.

First we model the low ionization phase. To constrain the nature of this phase we use column densities of C II, Si II, N II and Si III. The narrow H I component with higher N(H I) is associated with this low ionization gas. In panel-(a) of Fig. 2 we show the model results computed for $\log N$(H I) = 15.92$\pm$0.08. In this plot, different curve represents loci of different low ions in the metallicity – ionization parameter ($\log Z$ – $\log U$) plane. The (yellow) circle represents the area in the $\log Z$ – $\log U$ plane that is allowed by data. The model parameters are summarised in Table 2. Note that N II is consistent with this solution only if nitrogen is underabundant by a factor of $\sim$3. This low ionization phase also produce less N III (i.e. $\log N$(N III) = 12.45) and C III (e.g. $\log N$(C III) = 13.65) than observed. However, we could not confirm the presence of N III since the relevant wavelengths are severely affected by Geo-coronal Lyα emission. Also C III is an intermediate ion with contribution from both high and low ionization phases. This low ionization phase do not produce any significant high ion absorption, including Si IV.

Panel-(b) of Fig. 2 show the photoionization model for the high ionization phase of system **1A**. This phase is constrained by the column densities of C III, C IV, N V and O VI. Here we use corrected N(C III), obtained after dividing out the contribution of the low ionization phase from the C III profile. We associate the N(H I) as measured in the broad H I component (see Table 1) with the high ionization phase. This is a natural choice in view of the Broad Lyα Absorber (BLA) studies by Savage et al. (2011a,b, 2012); Narayanan et al. (2012), where diffuse gas traced by high ions (e.g. O VI), is usually associated with a broad Lyα absorption. In Table 2 photoionization model parameters are summarized. We notice that within the allowed ranges of $\log U$ and $\log Z$, this high ionization phase can produce significant amount of N III, (e.g. $\log N$(N III) = 13.50). But, we could not confirm it because of Geo-coronal

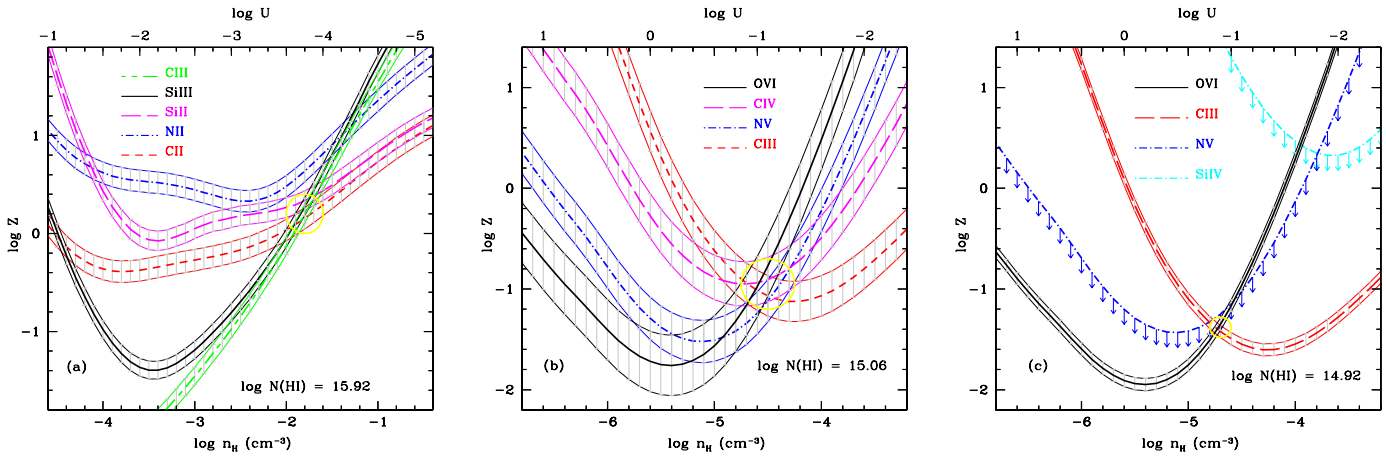

Figure 2. Photoionization models for the low ionization phase of system **1A** [panel-(a)], high ionization phase of system **1A** [panel-(b)] and system **1B** [panel-(c)]. Different curves showing loci of different ions in the $\log Z$ – $\log U$ plane for a given N(H I). The error in each curve is contributed by error in ionic and H I column density measurements. The (yellow) circle represents the allowed ranges in $\log U$ and $\log Z$.

Lyα emission as mentioned earlier. No singly ionized species or Si III, are produced in this phase. In passing, we wish to point out that the two weak H I components, at $v_{\rm rel} = -250$ and -400 km s^{-1}, show ranges in $\log U$ and $\log Z$ which are very similar to this high ionization phase.

3.2. *System at $z_{\rm abs} = 0.227$ towards* **B** *(system* **1B***)*

The velocity plot of this system is shown in the right panel of Fig. 1. Compared to system **1A**, this system show weaker H I absorption. No higher order Lyman series lines are detected beyond Lyδ. Lyα shows three components as also seen in system **1A**. Lyγ and Lyδ lines are blended with the Galactic Si IIλ1193 and O IIIλ832 absorption from $z_{\rm abs}$ = 0.39915 respectively. We have modelled out these blends while fitting. No metal line other than O VI and C III (only in one component) is detected in this system. The wavelengths redward to the detected C III is affected by the Galactic N Iλ1199 line. We note that O VI profile, albeit showing three components as Lyα, is not exactly aligned with Lyα profile. Similar to system **1A**, the O VI absorption here is also spread over $\sim$405 km s^{-1}. Si IV and N V transitions are covered by the COS spectrum, however, we do not detect any measurable absorption at the expected wavelengths. We estimate 3σ upper limits on N(N V) and N(Si IV) from the observed error spectrum (see Table 1). Since C III and O VI are detected only in the blue-most H I component (i.e. at $v_{\rm rel}\sim -120$ km s^{-1}) we use this component for photoionization modelling.

3.2.1. *Photoionization Model for system* **1B**

The photoionization model of the component at $v_{\rm rel}\sim -120$ km s^{-1} of this system is shown in panel-(c) of Fig. 2. We use H I, C III and O VI column density measurements and limits on N(N V) and N(Si IV) to constrain our model. The model parameters are summarized in Table 2. Note that the allowed values of $\log Z$ and $\log U$ are consistent with the non-detections of N V and Si IV. This single phase solution produces a C IV column density of $\log N$(C IV) = 13.67 corresponding to a $W_{\rm obs}$(1548) = 0.19 Å only. This is close to the detection threshold in the FOS/G190H spectrum and therefore consistent with there being no C IV equivalent width reported for this system in Crighton et al. (2010).

4. DISCUSSIONS AND CONCLUSIONS

Table 2
Model parameters in the $z_{\rm abs}$ = 0.227 systems towards **A** and **B**

System	$\log U$	$\log Z$	$\log N$(H) (N in cm^{-2})	$\log l^a_{\rm los}$ ($l_{\rm los}$ in kpc)
1A(Low)^b	-3.80 ± 0.20	0.20 ± 0.20	17.5 ± 0.2	-2.2 ± 0.4
1A(High)^c	-1.10 ± 0.25	-0.95 ± 0.25	19.6 ± 0.3	2.6 ± 0.5
1B	-0.90 ± 0.10	-1.38 ± 0.10	19.7 ± 0.1	2.9 ± 0.2

Notes – ^{a}size of the absorber along the line of sight. ^{b}parameters for low ionization phase. ^{c}parameters for high ionization phase.

We present analysis of two O VI absorbers (system **1A** and **1B**), detected in the spectra of two closely spaced QSOs (Q0107–025**A** and **B**), at redshift $z_{\rm abs}$ = 0.227. The angular separation between **A** and **B** (1.29 arcmin) corresponds to a transverse separation of $\sim$280 kpc at the absorber's redshift. At the same redshift, a single bright ($1.2L^\star$) galaxy at an impact parameter of $\sim$ 200 kpc (from both the sightlines **A** and **B**) was identified by Crighton et al. (2010). These authors have measured star formation rate (SFR) $>$ 0.45 M$_\odot$yr^{-1} and metallicity $\log Z \geq -0.30$ and claimed that the galaxy did not experience bursts of star formation within the last 2 Gyr. Nevertheless, the large velocity spreads (>400 km s^{-1}) of O VI absorption in both the systems possibly suggest that the highly ionized gas could originate from galactic winds/outflows. But, as there is no recent star formation activity in the candidate galaxy, it cannot be a fresh wind. Such an observation is consistent with the "ancient outflows" as predicted in a recent simulation by Ford et al. (2013). We note that a wind material moving with a speed of 100 km s^{-1} can reach a distance of $\sim$200 kpc in 2 Gyr time.

To understand the physical conditions in the absorbing gas we have built grids of photoionization models. We find that the strongest H I component in system **1B** can be explained with a single phase photoionization model, whereas, the strongest H I component in system **1A** required at least two phases to explain all the detected ions. Moreover, we find remarkable similarities between the photoionization model parameters of system **1B** and the high ionization phase of system **1A**. For example, they show ionization parameter, $\log U \sim -1.1$ to -0.9; metallicity, $\log Z \sim -1.4$ to -1.0; total hydrogen column density, $\log N_{\rm H}({\rm cm}^{-2}) \sim 19.6 - 19.7$ and line of sight thickness, $l_{\rm los} \sim 600 - 800$ kpc. All these suggest that the O VI absorption in systems **1A** and **1B** are

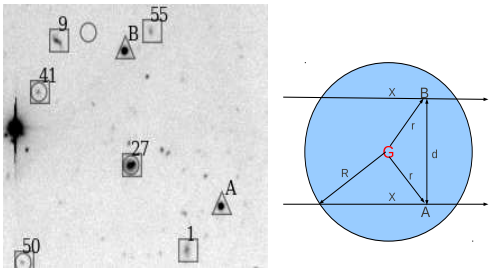

Figure 3. Left: Zoomed version of Fig. 1 of Crighton et al. (2010) showing image of the field. The box labelled as '27' is the candidate galaxy ∼200 kpc away from quasars **A** and **B** shown by triangles. The other boxes are galaxies which are not coincident with the absorber. Their galaxy sample is complete to an R band magnitude of ∼ 21. Right: Schematic diagram showing CGM of the galaxy with radius $R = \sqrt{(x/2)^2 + (d/2)^2}$. Here x and d are the line of sight thickness (∼ 600 kpc) and transverse separation between the absorbers (∼ 280 kpc) respectively.

possibly tracing the same large scale structure, presumably the CGM of the galaxy identified at the same redshift.

Fig. 3 shows the image of the field (left) and a schematic diagram of the CGM (right) as traced by O VI absorption. Using the estimated line of sight thickness and transverse separation between the two absorbers, we estimate size of the CGM, $R \sim 330$ kpc. Assuming the model-predicted density (i.e. $\log n_{\rm H} \sim -4.6$) is uniform inside the sphere of radius R, we find CGM mass to be $M_{\rm CGM} \sim 1.2 \times 10^{11} {\rm M}_{\odot}$[4]. Such a large mass in the ionized CGM is also reported by Tumlinson et al. (2011b); Tripp et al. (2011). However, all these studies assume some fiducial values of ionization correction and/or metallicity which are not well constrained by any detailed ionization models.

Our photoionization model suggests that the low ionization phase of system **1A** can produce $\log N({\rm Mg\,II}) = 12.87$. Therefore this system is a weak Mg II absorber candidate. This low ionization phase is compact in size ($l_{\rm los} \sim 6$ pc) and show high metallicity ($\log Z = 0.20 \pm 0.20$). Note that the metallicity is ∼10 times higher compared to that of the high ionization phase. Such near-solar metallicity and parsec scale size are very common features of weak Mg II absorbers (Rigby et al. 2002; Narayanan et al. 2008; Misawa et al. 2008). Moreover, Narayanan et al. (2008) have hypothesized that weak Mg II absorbers are likely to be tracing gas in the extended halos of galaxies, analogous to the Galactic HVCs. It is intriguing to note that this low ionization phase is detected only in system **1A** but not seen in system **1B**. Therefore we put forward a scenario where the low ionization phase traces high density pockets, like HVCs, and the high ionization phase traces extended and diffuse CGM gas. The density difference between the two phases is more than two orders of magnitude. Thus pressure equilibrium would require temperature difference to be of the same order. However, the photoionization temperatures are not that different between the two phases, suggesting that such an absorber could be short-lived.

[4] Note that the high ionization phase of system **1A** can also be explained with non-equilibrium collisional ionization models (Gnat & Sternberg 2007) with $\log T \sim 5.2$, $\log Z = -1.0$ and $\log N_{\rm H}({\rm cm}^{-2}) \sim 20.4$, provided nitrogen is underabundant by a factor of ≥5 (factor of ≥10 in the case of collisional ionization equilibrium). The estimated CGM mass in this case is $\sim 9.8 \times 10^{11} {\rm M}_{\odot}$. However, measured Doppler parameters of different species (e.g. b(N V) = 45±11 km s^{-1}, b(O VI) = 48±5 km s^{-1} and b(H I) = 48±4 km s^{-1}) do not support such a high temperature.

5. ACKNOWLEDGEMENTS

SM thanks Dr. Anand Narayanan, Dr. Raghunathan Srianand and Dr. Jane Charlton for useful discussions which improved the content significantly.

REFERENCES

Asplund, M., Grevesse, N., Sauval, A. J., & Scott, P. 2009, ARA&A, 47, 481
Bechtold, J., Crotts, A. P. S., Duncan, R. C., & Fang, Y. 1994, ApJ, 437, L83
Bouché, N., Dekel, A., Genzel, R., et al. 2010, ApJ, 718, 1001
Crighton, N. H. M., Morris, S. L., Bechtold, J., et al. 2010, MNRAS, 402, 1273
Davé, R., Finlator, K., & Oppenheimer, B. D. 2011a, MNRAS, 416, 1354
—. 2012, MNRAS, 421, 98
Davé, R., Oppenheimer, B. D., & Finlator, K. 2011b, MNRAS, 415, 11
Dekel, A., Birnboim, Y., Engel, G., et al. 2009, Nature, 457, 451
Dinshaw, N., Foltz, C. B., Impey, C. D., Weymann, R. J., & Morris, S. L. 1995, Nature, 373, 223
Dinshaw, N., Weymann, R. J., Impey, C. D., et al. 1997, ApJ, 491, 45
D'Odorico, V., Cristiani, S., D'Odorico, S., et al. 1998, A&A, 339, 678
Ferland, G. J., Korista, K. T., Verner, D. A., et al. 1998, PASP, 110, 761
Ford, A. B., Davé, R., Oppenheimer, B. D., et al. 2013, ArXiv e-prints, arXiv:1309.5951
Gnat, O., & Sternberg, A. 2007, ApJS, 168, 213
Green, J. C., Froning, C. S., Osterman, S., et al. 2012, ApJ, 744, 60
Haardt, F., & Madau, P. 1996, ApJ, 461, 20
Kacprzak, G. G., Churchill, C. W., Steidel, C. C., Spitler, L. R., & Holtzman, J. A. 2012, MNRAS, 427, 3029
Kereš, D., Katz, N., Weinberg, D. H., & Davé, R. 2005, MNRAS, 363, 2
Kriss, G. A. 2011, Improved Medium Resolution Line Spread Functions for COS FUV Spectra, Tech. rep.
Misawa, T., Charlton, J. C., & Narayanan, A. 2008, ApJ, 679, 220
Muzahid, S., Srianand, R., Bergeron, J., & Petitjean, P. 2012, MNRAS, 421, 446
Muzahid, S., Srianand, R., & Petitjean, P. 2011, MNRAS, 410, 2193
Narayanan, A., Charlton, J. C., Misawa, T., Green, R. E., & Kim, T.-S. 2008, ApJ, 689, 782
Narayanan, A., Savage, B. D., & Wakker, B. P. 2010, ApJ, 712, 1443
—. 2012, ApJ, 752, 65
Oppenheimer, B. D., Davé, R., Kereš, D., et al. 2010, MNRAS, 406, 2325
Osterman, S., Green, J., Froning, C., et al. 2011, Ap&SS, 335, 257
Petry, C. E., Impey, C. D., Fenton, J. L., & Foltz, C. B. 2006, AJ, 132, 2046
Rauch, M., Sargent, W. L. W., & Barlow, T. A. 2001, ApJ, 554, 823
Rigby, J. R., Charlton, J. C., & Churchill, C. W. 2002, ApJ, 565, 743
Savage, B. D., Kim, T.-S., Keeney, B., et al. 2012, ApJ, 753, 80
Savage, B. D., Lehner, N., & Narayanan, A. 2011a, ApJ, 743, 180
Savage, B. D., Narayanan, A., Lehner, N., & Wakker, B. P. 2011b, ApJ, 731, 14
Savage, B. D., Sembach, K. R., Wakker, B. P., et al. 2003, ApJS, 146, 125
Sembach, K. R., Wakker, B. P., Savage, B. D., et al. 2003, ApJS, 146, 165
Springel, V., & Hernquist, L. 2003, MNRAS, 339, 289
Stocke, J. T., Keeney, B. A., Danforth, C. W., et al. 2013, ApJ, 763, 148
Thom, C., & Chen, H.-W. 2008, ApJS, 179, 37
Thom, C., Tumlinson, J., Werk, J. K., et al. 2012, ApJ, 758, L41
Tripp, T. M., Sembach, K. R., Bowen, D. V., et al. 2008, ApJS, 177, 39
Tripp, T. M., Meiring, J. D., Prochaska, J. X., et al. 2011, Science, 334, 952
Tumlinson, J., Werk, J. K., Thom, C., et al. 2011a, ApJ, 733, 111
Tumlinson, J., Thom, C., Werk, J. K., et al. 2011b, Science, 334, 948
Wakker, B. P., & Savage, B. D. 2009, ApJS, 182, 378
Werk, J. K., Prochaska, J. X., Thom, C., et al. 2013, ApJS, 204, 17
Young, P. A., Impey, C. D., & Foltz, C. B. 2001, ApJ, 549, 76